GRANULATION and FIVE–MINUTE OSCILLATIONS

E. V. Khomenko, R. I. Kostik, and N. G. Shchukina

Main Astronomical Observatory, NAS of Ukraine
27 Zabolotnoho St., 03680 Kyiv, Ukraine
e-mail: `kostik@mao.kiev.ua`

We discuss the links between the photospheric 5–min oscillations and granulation patterns using a 30-min time series of CCD spectral images of solar granulation recorded with high spatial (0.″5) and temporal (9.3 s) resolution. The observed images contain Fe I 5324 Å line. Our observations and theoretical modeling lead to the similar results: (i) period of oscillations varies above granules and lanes; (ii) amplitudes of the velocity oscillations grow with the contrast of granulation. Amplitudes of the intensity oscillations are larger in intergranular lanes than in granules. Our simple model describes the basic features of the oscillations above granules and intergranular lanes. We conclude that differences in these oscillations are caused mainly by variations of the physical conditions in these structures.

INTRODUCTION

Spatial relation between the 5–min oscillations and granulation patterns is much debated in the literature. Most support theoretical suggestions made by Goldreich, Keeley, Kumar, and Murray [5]–[7], [14] that acoustic waves which comprise the observed 5–min oscillations are stochastically generated by turbulent convection just beneath the photosphere. Moreover, Brown [3] predicted that the most of the acoustic emission should come from rare localized events, where convective velocities are the highest. Goode, Gough, and Kosovichev [8] associate these localized events with expanding overshooting granules.

Recent study of the spatial relation between the solar granulation and the 5–min oscillations completed by Espagnet *et al.* [4] confirms that the strong oscillations are well isolated temporally and spatially. However, the most energetic oscillations turned out to occur only in expanding intergranular spaces with the strong downflows. This conclusion disagrees with the picture in which the oscillations are excited by expanding overshooting granules. On the other hand, analyzing G-band granulation filtergrams Hoekzema *et al.* [9]–[11] have deduced “that the photospheric 5–min oscillations are primarily global and rather insensitive to the local fine structure”.

We conclude that despite considerable efforts by various researchers the issue of the links between the 5–min oscillations and granulation remains open.

OBSERVATIONS AND DATA REDUCTION

The observations were carried out with the 70-cm German Vacuum Tower Telescope at the Observatorio del Teide, Tenerife, in August 1996. The telescope and spectrograph are described by Schröter *et al.* [21]. The CCD images contain the photospheric Fe I 5324 Å line. The observed area was placed near the quiet solar disk centre. Magnetically active regions were avoided by controlling the entrance slit position using H_α and Ca II K slit–jaw images. We used CCD camera with 1024×1024 pixels, in 2×2 binning mode. A pixel size in this mode was 0.174 arcsec in the spatial direction. The dispersion of the spectra was of about 0.10 Å/mm at 6000 Å. The entrance slit width of the spectrograph was set to 80 μm, *i.e.*, 0.38 arcsec on the solar disk. Thus, each overall image corresponds to an area on the solar surface of about 0.38×89 arcsec^2. The Fe I 5324 line spectrograms were taken every 9.3 s with integration time 5.7 s. The time series covered about 31 minutes and included 200 images in total.

The reduction of CCD images followed the standard procedure. For each averaged spectral pixel row i ($i = 1 - 170$) of each image j ($j = 1 - 200$) we inferred intensity and velocity signals at 11 levels of the line profile $\delta I_l(i,j)$, (l = 0 − 10) and $\delta V_l(i,j)$, (l = 0 − 10), where $l = 0$ corresponds to the line core. The procedure was performed applying the method described by Stebbins and Goode [23].

Invited paper.

The variations in the line parameters under study are induced mainly by convective and wave motions. In order to separate granular and oscillatory components of the velocity field we constructed a diagnostic $k - \omega$ diagram.

RESULTS AND DISCUSSION

"Artificial granule", power–contrast diagram

One of the ways to investigate the links between the 5–min oscillations and granulation is to isolate an individual granule and intergranular lane and then to observe the evolution of oscillations above them. However, there are two problems:

- How to identify the same granulation structure during its lifetime?
- How to apply the methods of spectral analysis to such a short time series (granular mean lifetime is ~ 10 min according to Title *et al.* [24]?

To overcome the problem we constructed an "artificial" spectrum of granule and intergranular lane and followed its evolution in time (the method firstly applied by Kostik and Shchukina [12]). According to this approach we splitted spectral rows of each image into granular and intergranular ones using the spatially and temporally averaged continuum intensity $\bar{I}_c$ as the criterion. Having averaged separately the spectra of the rows with positive and negative contrast in each image we obtained two time sequences, one of which contained only the averaged granule spectra and the other – the averaged intergranular spectra. Following that way we introduced more refined classification of the continuum contrast differences. The bright and dark samples were splitted further into 6 contrast classes by combining the rows in the same class if its contrast exceeded some threshold. We used thresholds for the granular rows in the range $1 - 5.5\%$ and for the intergranular ones in the range from -1% to -5%.

Figure 1 displays the power–contrast $(P - I)$ diagram for the "artificial" granular pattern. Left-hand side panels in Fig. 1 represent observational results while right-hand side ones represent simulations. We will discuss the simulations in the next Subsection. Now we refer only to observations. In the diagram, the power of the central residual intensity δI_{0W} (panel a) and velocity δV_{0W} (panel c) oscillations are plotted against the normalized continuum contrast δI_c. In our observations the greatest power concentrates at two frequencies: $\omega = 3.73 \pm 0.26$ and $\omega = 3.21 \pm 0.26$ mHz (the periods are equal to 268 and 312 s, respectively). At the period $T = 268$ s there is much more power of velocity oscillations in the negative range of contrast than in the positive one. Contrary to that, at the period $T = 312$ s the power is distributed over the whole range of granulation contrast, but there is less power in the negative range. Around this period the power increases with absolute value of the contrast: strong velocity oscillations occur preferentially above the brightest granules (where the power is the maximum) and above the darkest intergranular lanes. Thus, we conclude that the powerful velocity oscillations may be found above granules as well as above intergranular lanes, but with different periods. These results disagree with Espagnet *et al.* [4] who argue that the most energetic velocity oscillations occur only above intergranules.

The power of the intensity oscillations δI_{0W} has another distribution (Fig. 1c). It increases with contrast both above granules and intergranules but the most energetic intensity oscillations are present only above intergranules. This is correct for oscillations with 268 and 312 s periods. Unfortunately, we cannot compare these results with those of Espagnet *et al.* [4] because the authors do not provide the corresponding data.

Simulation of the wave propagation in the photosphere

It seems natural that oscillations above granules and intergranular lanes are not identical because the physical conditions in these regions vary a lot. Even under assumption that oscillations at the bottom are generated with equal amplitudes, dissimilarities should occur at the top of the photosphere if they propagate through a considerably different media such as granules and intergranular lanes. Firstly, temperature is not the same in granules and intergranules. Intergranules have less steep temperature gradient and are cooler in the deeper layers, while granules become cooler in the upper layers of the atmosphere. This conclusion is supported by numerous observational studies among of which are the recent results by Rodríguez Hidalgo *et al.* [17], who applied an inversion code to high quality two-dimensional spectroscopic data and extracted information about temperature and other parameters of granular/intergranular atmospheres. Theoretical simulations of solar granulation also demonstrate the same tendency (see for example the paper by Asplund *et al.* [1]). Temperature variations act on the radiative relaxation time. The oscillations are very sensitive to the latter. Changes in temperature also modify the acoustic cut-off frequency under which the oscillations are actively damped. Secondly, differences in pressure and density affect the scale height to which an oscillatory amplitude is sensitive. And the least but not the last, oscillations propagate in a moving medium with upflows, downflows and horizontal flows. This should modify their propagation frequency and affect the phase shifts simply because of the Doppler effect.

Regarding to the aforementioned considerations, we found it reasonable to reconsider the theory of wave propagation in the solar atmosphere and to pay more attention to the effect of oscillations on a line profile. The main difference between our work and similar studies of other authors (*e.g.*, [2, 15, 16] and references therein) is that we considered wave propagation in a moving medium. In all the cited papers, the granulation component of the velocity field was neglected and only oscillatory perturbations were considered. In the present study we make an attempt to include both velocity components.

A comprehensive analysis of the propagation of the acoustic-gravity waves in a radiating fluid is fulfilled by Mihalas and Mihalas [18]. We follow this analysis and the scheme given by Noyes and Leighton [19] and then developed by Kostik [13] and Schmieder [20]. We solved analytically the hydrodynamical equations of mass, momentum and energy conservation:

$$\rho\frac{d\vec{V}}{dt} = -\vec{\nabla}P + \vec{g}\rho\,; \tag{1}$$

$$\frac{\partial\rho}{\partial t} = -\vec{\nabla}(\rho\vec{V}); \tag{2}$$

$$\frac{dQ}{dt} = c_v\frac{dT}{dt} - \frac{RT}{\rho}\frac{d\rho}{dt}, \tag{3}$$

where d/dt is the Stokes derivative, dQ/dt is the net rate of radiative energy input (per unit volume) to the gas from external sources; other notations are standard. We assumed that there are no magnetic field; viscosity and thermal conduction terms can be omitted; the effects of solar rotation are negligible; to the 0^{th} order, the atmosphere is plane parallel, horizontally homogeneous and in radiative equilibrium. The matter is described by a suitable equation of state (no effects of ionization are considered):

$$\frac{T_1}{T_0} = \frac{P_1}{P_0} - \frac{\rho_1}{\rho_0}. \tag{4}$$

The effects of radiative relaxation, the main source of dissipation for linear waves in the solar photosphere, is taken into account by using the Newtonian cooling approximation. The motion is restricted to one dimension, hence, internal gravity waves are excluded from consideration. Solution of the system of partial differential equations was obtained by approximating the atmosphere as a series of isothermal layers each of a given thickness (10 km) moving with a constant velocity. In each layer we linearized the fundamental equations with:

$$T = T_0 + T_1, \quad P = P_0 + P_1, \quad \rho = \rho_0 + \rho_1, \quad V = V_0 + V_1. \tag{5}$$

The dimensionless and linearized equations then become (to the 1^{st} order):

$$\frac{\partial W_1}{\partial t} + W_0\frac{\partial W_1}{\partial z} = -\frac{\partial}{\partial z}(R+\Theta) + 2\Theta\,; \tag{6}$$

$$\frac{\partial R}{\partial t} + W_0\frac{\partial R}{\partial z} = 2W_0R - \frac{\partial W_1}{\partial z} + 2W_1; \tag{7}$$

$$\frac{\partial\Theta}{\partial t} + W_0\frac{\partial\Theta}{\partial z} = -\frac{1}{\tau_{RR}}\Theta - (\gamma-1)\frac{\partial W_1}{\partial z}. \tag{8}$$

Here the vertical velocity W is measured in a units of acoustic velocity ($W_{0,1} = V_{0,1}/C_s$), values $\Theta = T_1/T_0$ and $R = \rho_1/\rho_0$ – in a units of the corresponding unperturbed values, distance $z = \tilde{z}/2H$ – in a units of the doubled pressure scale height $H^{-1} = -\nabla P/P$ at the given layer. The system has an exponential solution at the fixed frequency of the form:

$$W_1,\,\Theta,\,R \sim e^{z(1-k_i)}e^{-ik_r(tV_{ph}-tW_0-z)}, \tag{9}$$

where $V_{ph} = \omega/k_r$ is a phase velocity of the wave, k_r and k_i are the real and imaginary parts of the vertical wave number k_z. Only upward modes can be excited in an isothermal atmosphere perturbed from below; therefore, by selecting an upward solution of the Eqs. (6)–(8), the vertical velocity can be written as follows:

$$W_1 = V_{0w}e^{z(1-k_i)}\sin((\omega - W_0k_r)t - k_rz). \tag{10}$$

The corresponding waveform for the thermodynamic perturbations T_1/T_0 and ρ_1/ρ_0 were obtained from the polarization relations and the pressure perturbations was found from the equation of state (see Eq. (4)):

$$\frac{T_1}{T_0} = |\Theta| e^{z(1-k_i)} \sin((\omega - W_0 k_r)t - k_r z + \phi_{TV}), \tag{11}$$

$$\frac{\rho_1}{\rho_0} = |R| e^{z(1-k_i)} \sin((\omega - W_0 k_r)t - k_r z + \phi_{\rho V}). \tag{12}$$

Variations of the thermodynamical quantities (see Eqs. (10)–(12)) were introduced in the model atmosphere and then profiles of the Fe I 5324 Å line were synthesized.

Note that positive direction of the vertical axis z in our study was chosen toward to the centre on the Sun, thus, waves moving toward the observer have negative velocity. Note also that since we have a non-zero vertical velocity field, the effective frequency which we can measure is not constant now, but is modified by velocity:

$$\tilde{\omega} = \omega - W_0 k_r. \tag{13}$$

To study peculiarities of the wave propagation above granules and intergranular lanes an appropriate model atmosphere is desired. In the present study we utilized a snapshot of the 3D model atmosphere from the most recent numerical simulations by Asplund *et al.* [1]. We used simulations with resolution of $50 \times 50 \times 82$ grid-points corresponding to the physical dimension of $6.0 \times 6.0 \times 3.8$ Mm with nearly 1.0 Mm being located above the continuum optical depth unity. The simulated box includes about 15 granules. We considered the 3D snapshot as a set of 1D granular/intergranular model atmospheres. For the line profiles calculations we randomly chose a slice from the snapshot which contains 5 granules separated by intergranular lanes.

For each such a model we computed the line intensity using the formal solution of the time–dependent radiative transfer equation for the case of the moving atmosphere perturbed by oscillations. We used as input in formal radiative transfer solution NLTE departure coefficients found from the self–consistent solution of the kinetic and radiative transfer equations for the realistic iron atomic model and unperturbed granulation models. We assume that perturbations caused by wave in the atmosphere are small enough so the departure coefficients do not change in the perturbed model atmosphere. All details of our NLTE computations are described by Shchukina and Trujillo Bueno [22]. Time series of 40 profiles with the real time step of 9.3 sec, close to the observed value, were synthesized in each of the 50 models. The overall time of computations was about 1 wave period ($\sim$ 5 minutes). Initial amplitude of the wave perturbation was chosen equal to $V_0 = 100$ m s^{-1}, and two sets of the profiles were calculated, one with the initial period of the wave 312 s and another with 268 s. The value $V_0 = 100$ m s^{-1} was taken from our observations of the spatially averaged oscillations at height $H = 0$ km. We solved an inverse problem and restored oscillations of intensity and velocity at 11 levels of the computed line profiles applying the same method as for the observational data.

Figure 1b and 1d represent the $P - I$ diagram, computed using theoretical profiles. As before we separated profiles into 14 contrast classes and ascribed profile to a certain class if its continuum contrast has been higher (for granules) or lower (for lanes) than some threshold. Curves for two initial periods ($T = 268$ and 312 s) are shown.

In general, theoretical $P - I$ diagram resembles the main features of the observed diagram. This supports the conclusion by Kostik and Shchukina [12] showing that observed increase of power of oscillations above the most contrast space is not an artifact due to averaging of the spectral profiles over areas of different size, but is a real effect. We see that theory also gives a rapid increase of power of oscillations above intergranular lanes, both for intensity and, in a less degree for velocity. Above granules there are much less power for both periods of oscillations. The difference in power between two periods (268 and 312) is more or less the same both in observations and theory: oscillations with period 268 s are more powerful.

Nevertheless, there is an important difference between observed and simulated $P - I$ diagram. Observed oscillations above the low-contrast space have a very little power, it is nearly zero for period 312 s, while simulated oscillations do not exhibit the tendency.

Another important discrepancy is the rapid increase of the velocity power above granules for the period $T = 312$ s. Theory does not explain why velocity oscillates with larger period above granules than above intergranular lanes. Probably, it may be attributed to the second-order effects which are not taken into account by the linear theory we have employed.

CONCLUSIONS

The observations with high spatial ($< 0''.5$) and temporal (9.3 s) resolution and a new method have allowed us to investigate in details the local 5–min oscillations above granules and intergranules. In the upper photosphere

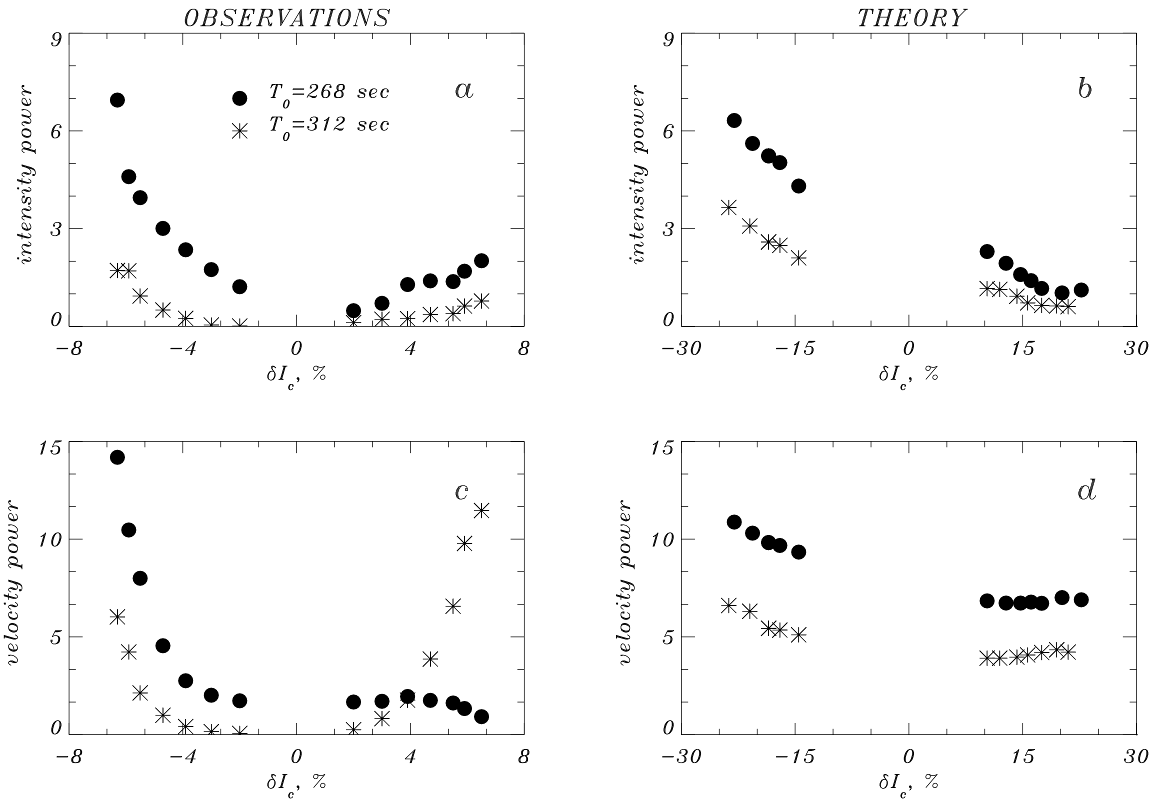

Figure 1: **a** and **b**: power of the intensity oscillations of the line core as a function of the normalized continuum contrast δI_c. **c** and **d**: the same but for velocity oscillations Results for two periods with the maximum power in a spectrum are shown. Filled circles: period 268 s; stars: 312 s. Units for intensity and velocity power are $[\delta I_{0W}/\bar{I}_c]^2$ and $[ms^{-1}]^2 \times 10^{-4}$, respectively. For details see discussion in the text

at a height $\sim$ 500 km, the average amplitudes of velocity oscillations above granules are lower than above intergranules. The main power of the velocity fluctuations concentrates at the frequencies $\omega = 3.21 \pm 0.26$ mHz (T = 312 s) and $\omega = 3.73 \pm 0.26$ mHz (T = 268 s). Power of the velocity oscillations with T = 312 s reaches maximum above the bright areas (granules) while power of oscillations with T = 268 s has maximum above the dark intergranular lanes. The main power of the intensity fluctuations concentrates only at $\omega = 3.21 \pm 0.26$ mHz, and above intergranules it is a factor of 3 higher than above granules.

Acknowledgements. Partial support by the Spanish DGICYT under project 91–0530 is gratefully acknowledged. N. G. S. would like to acknowledge the support of the Spanish Ministry of Education for a sabbatical stay at the IAC. The support provided by C. Briand and H. P. Schilling during the observations is gratefully appreciated. We would like to thank M. Vázquez, J. A. Bonet, J. Trujillo Bueno, M. Collados and their colleagues for support, interest and help in our work. Special thanks to M. Asplund for the kind permission to use 3D model atmosphere for the purposes of our study. We are grateful to A. Kosovichev for useful suggestions. We acknowledge support from the Netherlands Organization for Scientific Research (NWO). In this research, we employed in Kyiv a computer (CCD system) funded by the NWO.

REFERENCES

[1] *Asplund M., Nordlund A., Trampedach R., et al.* Line formation in solar granulation. I. Fe line shapes, shifts and asymmetries // Astron. and Astrophys.–2000.–**359**, N 2.–P. 729.

[2] *Bertello L., Caccin B.* Non–adiabatic modelling of "5–min" oscillations: effects on photospheric line profiles // Astron. and Astrophys.–1990.–**231**, N 2.–P. 509–517.

[3] *Brown T. M.* Excitation of the solar p-modes by turbulent stress // Astrophys. J.–1991.–**371**, N 1.–P. 396–403.

[4] *Espagnet O., Muller R., Roudier T., et al.* Spatial relation between the 5-minute oscillations and granular patterns // Astron. and Astrophys.–1996.–**313**, N 1.–P. 297–305.

[5] *Goldreich P., Keeley D. A.* Solar seismology. I. The stability of the solar p-modes // Astrophys. J.–1977.–**211**, N 3.–P. 934–942.

[6] *Goldreich P., Murray N., Kumar P.* Excitation of solar p-modes // Astrophys. J.–1994.–**424**, N 2.–P. 466–479.

[7] *Goldreich P., Kumar P.* The interaction of acoustic radiation with turbulence // Astrophys. J.–1988.–**326**, N 1.–P. 462–468.

[8] *Goode P. R., Gough D., Kosovichev A.* Localized excitation of solar oscillations // Astrophys. J.–1992.–**387**, N 2.–P. 707–711.

[9] *Hoekzema N. M., Brandt P. N., Rutten R. J.* Small scale topology of solar atmospheric dynamics III. Granular persistence and photospheric wave amplitudes // Astron. and Astrophys.–1998.–**333**, N 1.–P. 322–332.

[10] *Hoekzema N. M., Rutten R. J.* Small scale topology of solar atmospheric dynamics II. Granulation, K2ν grains and waves // Astron. and Astrophys.–1998.–**329**, N 2.–P. 725–734.

[11] *Hoekzema N. M., Rutten R. J., Brandt P. N.* Small scale topology of solar atmospheric dynamics I. Wave sources and wave diffraction // Astron. and Astrophys.–1998.–**329**, N 1.–P. 276–290.

[12] *Kostik R., Shchukina N.* Local 5–min oscillations above solar granules and intergranular space // Astron. Lett.–1999.–**25**, N 10.–P. 678–687.

[13] *Kostik R. I.* Influence of the running sound wave on the spectral line profiles. IV. Fe line shifts in the spectrum of the solar disc centre // Astrometriya i Astrofisica.–1974.–**23**, N 1.–P. 52–56.

[14] *Kumar P., Goldreich P.* Nonlinear interactions among solar acoustic modes // Astrophys. J.–1989.–**342**, N 2.–P. 558–575.

[15] *Marmolino C., Severino G.* Phases and amplitudes of acoustic–gravity waves. I. Upward and downward solutions // Astron. and Astrophys.–1991.–**242**, N 1.–P. 271–278.

[16] *Marmolino C., Stebbins R. T.* Wave behavior in the solar photosphere: a comparison of theory and observations // Solar Phys.–1989.–**124**, N 1.–P. 23–36.

[17] *Rodríguez Hidalgo I., Ruiz Cobo B., Collados M.* Granular and intergranular model atmospheres from inversion of solar two–dimensional spectroscopic data // Theory and tests of convection in stellar structure / Eds A. Giménez, E. F. Guinan, B. Montesinos.–ASP Conf. Ser.–1999.–**173**.–P. 313–317.

[18] *Mihalas D., Mihalas B. W.* Foundations of Radiation Hydrodynamics.–Oxford: Oxford Univ. press, 1984.–718 p.

[19] *Noyes R. W., Leighton R. W.* Velocity fields in solar atmosphere. II. The oscillatory field // Astrophys. J.–1963.–**138**, N 2.–P. 631–647.

[20] *Schmieder B.* Linear hydrodynamical equations coupled with radiative transfer in a non-isothermal atmosphere // Solar Phys.–1977.–**54**, N 1.–P. 269–288.

[21] *Schröter E. H., Soltau D., Wiehr E.* The German solar telescopes at the Observatorio del Teide // Vistas in Astronomy.–1985.–**28**, N 2.–P. 519–525.

[22] *Shchukina N. G., Trujillo Bueno J.* Fe I lines in spectra of cool stars: NLTE effects in solar-like atmosphere // Kinematics and Physics of Celestial Bodies.–1998.–**14**, N 4.–P. 315–329.

[23] *Stebbins R. T., Goode P. R.* Waves in the solar photosphere // Solar Phys.–1987.–**110**, N 1.–P. 237–253.

[24] *Title A. M., Tarbell T. D., Topka K. P., et al.* Statistical properties of solar granulation derived from the SOUP instrument on Spacelab 2 // Astrophys. J.–1989.–**336**, N 2.–P. 475–494.